

Analysis of Copper Incorporation into Zinc Oxide Nanowires

Susie Eustis, Douglas C. Meier, Michael R. Beversluis, and Babak Nikoobakht*

Surface and Microanalysis Science Division, National Institute of Standards and Technology, 100 Bureau Drive, Mail Stop 8372, Gaithersburg, Maryland 20899

ABSTRACT ZnO nanowires (NWs) are grown on a bulk copper half-transmission electron microscopy grid by chemical vapor deposition in a high temperature tube furnace. Photoluminescence (PL) microscopy revealed band gap emission at 380 nm and a more intense visible emission around 520 nm due to defect states in these NWs. High-resolution transmission electron microscopy shows that the ZnO NWs are single crystalline with hexagonal structure. Auger electron spectroscopy (AES) and energy dispersive X-ray spectroscopy reveal that copper atoms are present along the length of the NW. AES also found that the surface of the NWs is oxygen rich. The surface concentration of zinc increases moving from the tip toward the base of the NW while the concentration of oxygen decreases. The copper in this system not only remains at the tip of the growing NW but also acts as a dopant along the length of the NW, leading to a decrease in the intensity of the band gap PL of these NWs.

KEYWORDS: copper · microbeam analysis · nanotechnology · nanowires · photoluminescence · structural characterization · zinc

Zinc oxide (ZnO) nanostructures have received a lot of attention lately due to their photoluminescence (PL),^{1–4} field emission,⁵ and piezoelectric properties.^{6,7} The one-dimensionality of these structures leads to some of their interesting properties, along with the potential for novel applications. ZnO nanowires (NWs),^{3,8–10} nanobelts,¹¹ tetrapods,^{12,13} nanocombs,¹⁴ and many other shapes have been generated using high-temperature growth methods.² These nanostructures are potential candidates for UV light sources, sensors,¹⁵ solar cells,¹⁶ field emission sources,⁵ and piezoelectric devices.⁶

The lasing capabilities of single ZnO NWs offers promise for future technologies.^{1–4} However, the PL of ZnO NWs differs depending upon the synthesis method and the defects present in the sample. Usually two peaks are observed, one in the visible region (≈ 520 nm) and one in the UV region (≈ 380 nm).² The UV emission, referred to as the band gap emission, is observed at the energy corresponding to the difference between the conduction band and valence band electrons. The visible luminescence,

referred to as the deep trap emission, is believed to be due to one or more of the following causes: oxygen vacancies, adsorbed oxygen molecules, surface defects, and impurities that give rise to electron density in gap states. The presence of copper has been reported to increase the intensity of deep trap emission of bulk ZnO¹⁷ as well as the intensity of band gap emission of ZnO NWs.^{18–20} Li *et al.*¹⁸ showed that a copper catalyst generates ZnO NWs with more intense band gap emission than those generated from a gold catalyst. Xu *et al.*²⁰ observed a larger intensity band gap emission from NWs grown with a copper catalyst than nanostructures grown without a catalyst. Due to the potential applications of copper-doped and copper-catalyzed NWs in optoelectronic devices, the study of the distribution of copper atoms within ZnO NWs and their oxidation state becomes important. This could increase the understanding of the PL properties of copper-doped ZnO NWs by separating the effects arising from surface and bulk defects.

Previous studies have shown that copper catalyzes the growth of ZnO NWs via the vapor–liquid–solid (VLS) mechanism at high temperature.^{18–26} In the VLS mechanism, the metal forms a liquid droplet which sequesters zinc and oxygen precursor vapors, depositing ZnO on the surface.^{22,26–31} The NWs grow by the successive crystalline deposition of ZnO from the droplet, while the liquid metal droplet remains at the tip of the NW, as shown schematically in Figure 1a. Many researchers have shown the VLS mechanism to be a kinetic process where incorporation of the growth material into the droplet and into the growing NW depends on a number of parameters including the temperature history of the sample.^{28–30} Chemical properties also af-

*Address correspondence to
babak.nikoobakht@nist.gov.

Received for review October 29, 2007
and accepted December 21, 2007.

Published online January 12, 2008.
10.1021/nn700332r CCC: \$40.75

This article not subject to U.S. Copyright. Published
2008 by the American Chemical Society.

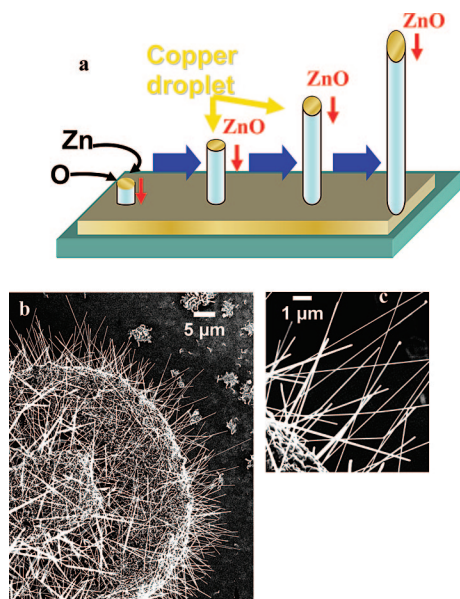


Figure 1. (a) Schematic drawing of VLS growth of ZnO NWs on copper. The copper acts as the catalyst where the Zn and O incorporate into the copper droplet to precipitate out as ZnO, growing the NW. (b and c) SEM images of ZnO NWs grown on a copper support where the copper droplets can be seen on the tips of ZnO NWs.

fect the properties of nanowires generated such as the vapor pressure of the source material,^{28,30,31} the solid/solid³² and liquid/solid³² solubility of the catalyst, and the growth material. Changing the synthesis conditions can influence the properties of the NWs formed as well. For example, increasing the temperature of ZnO NW growth, and thus increasing the rate of growth, leads to an increase in the deep trap emission.²⁹

Recently, spectroscopic techniques for compositional analysis have been applied to ZnO NWs. Previous Auger electron spectroscopy (AES) results for ZnO NWs grown at high temperature have shown roughly a 1:1 ratio of zinc to oxygen atoms, with carbon as the only impurity detectable.^{18,21,33} Complementary energy dispersive X-ray spectroscopy (EDS) results have also confirmed the presence of Zn and O in the NWs, as well as some impurities from the growth procedure (e.g., Si and the metal catalyst).^{21,24,25,34,35}

In this study, an analysis of the trace copper constituent has been carried out at the single NW level, both at the tip and along the body of the NW. The structure of the ZnO NW is probed with transmission electron microscopy (TEM), scanning electron microscopy (SEM), and X-ray diffraction (XRD), while the NW composition is determined using AES and EDS. As a complementary technique, the PL properties of ZnO NWs are investigated here, due to their strong variation with copper presence.^{17–20} EDS and AES on individual NWs show that during the growth process, copper is incorporated along the length of the NW. The strong deep trap PL of the ZnO NWs further confirms this finding.

RESULTS AND DISCUSSION

Scanning electron micrographs of ZnO NWs on a copper substrate are shown in panels b and c of Figure 1. The NWs' growth dimensions range from 50 to 150 nm in width and from 5 to 15 μm in length. The NWs grow in all directions from the copper surface. The copper droplet observed at the tip of the NW confirms that these NWs grow by the VLS mechanism.

Figure 2a shows a high-resolution TEM (HR-TEM) image where the single crystal nature of the NWs grown is observed. The individual atoms can be clearly seen in this image; the direction of growth is $[10\bar{1}1]$. Other NWs investigated with HR-TEM show the same single-crystalline structure regardless of the growth direction relative to the substrate. In order to further characterize the ZnO NWs grown on a copper substrate, XRD was used to determine the crystalline phase of the product. Figure 2b shows the XRD spectrum where the lattice planes of ZnO are all detected, along with the reflections from the copper substrate. The spectrum matches the lattice spacing of ZnO in the wurtzite structure, with a slight overexpression of the (002) plane suggesting a slight preference for that growth direction for some of the NWs. Peaks in the XRD spectrum for Cu_2O are also detected in this sample, due to the oxidation of the copper surface at high temperature. The $(\text{Cu}^+)_{2}\text{O}$ dominates at the high temperatures used in this growth procedure, while $(\text{Cu}^{2+})_{2}\text{O}$ is the more common form of copper oxide produced at lower temperatures.³⁶ The XRD results confirm the HR-TEM results, where the ZnO NWs show single crystal growth with multiple crystallographic directions observed for the growth directions of different nanowires.

The PL spectra of the ZnO NWs shown in Figure 3 are measured using a microspectrometer. The PL spectrum is uniform across the whole copper grid with band gap emission at 380 nm and more intense deep trap emission with a maximum around 520 nm. The deep trap emission dominates the emitted light as observed in this spectrum. Control PL experiments of the oxidized copper grid showed no emission due to the grid. Previous studies of uncatalyzed ZnO nanostructures showed that deep trap emission due to adsorbed oxygen molecules or dust particles on the NW surface can be decreased by submerging the ZnO NWs in ethanol.³⁷ Figure 3 shows the PL spectrum of the same location while immersed in ethanol. The intensity of the deep trap emission and the band gap emission decreased while immersed in ethanol. In order to adjust the spectrum for the difference in refractive index of ethanol *versus* air and for variation in scattering, the spectra are normalized to the band gap emission in Figure 3b. A relative decrease in the intensity of the deep trap emission is observed while in ethanol; however, normalized spectra of these NWs submerged in water showed no change. After the etha-

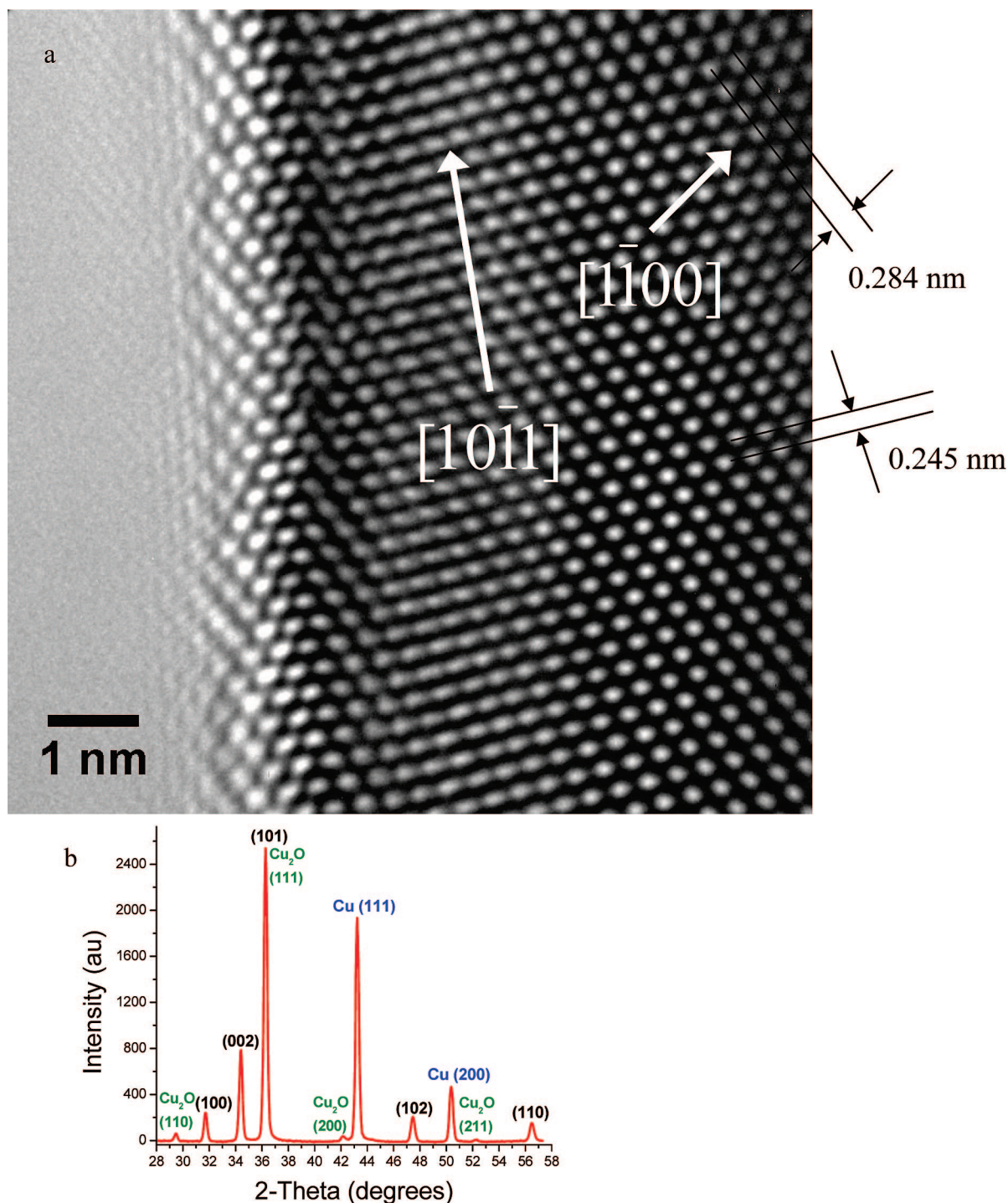


Figure 2. (a) High-resolution TEM image of a single crystal ZnO NW growing in the $[10\bar{1}1]$ direction. (b) XRD spectrum of ZnO NWs on a copper grid showing the characteristic crystal planes of ZnO (black), copper (blue), and copper oxide (green). The NWs grow in multiple crystallographic directions.

nol evaporates, the emission spectrum returns to that observed originally, and this change with ethanol presence and absence is repeatable (data shown in Figure S-1, Supporting Information). This decrease in intensity of the deep trap emission is not accompanied by an increase in intensity of the band gap emission due to ethanol presence nor does the deep trap emission disappear completely. Therefore,

ethanol quenches the PL due to the surface defect states of these ZnO NWs while in suspension, presumably through nonradiative recombinations. Nonradiative recombinations have previously been attributed to Zn vacancies in ZnO crystals affecting both the band gap emission and the deep trap emission.³⁸ There are other electron traps present in these NWs responsible for the weak band gap emis-

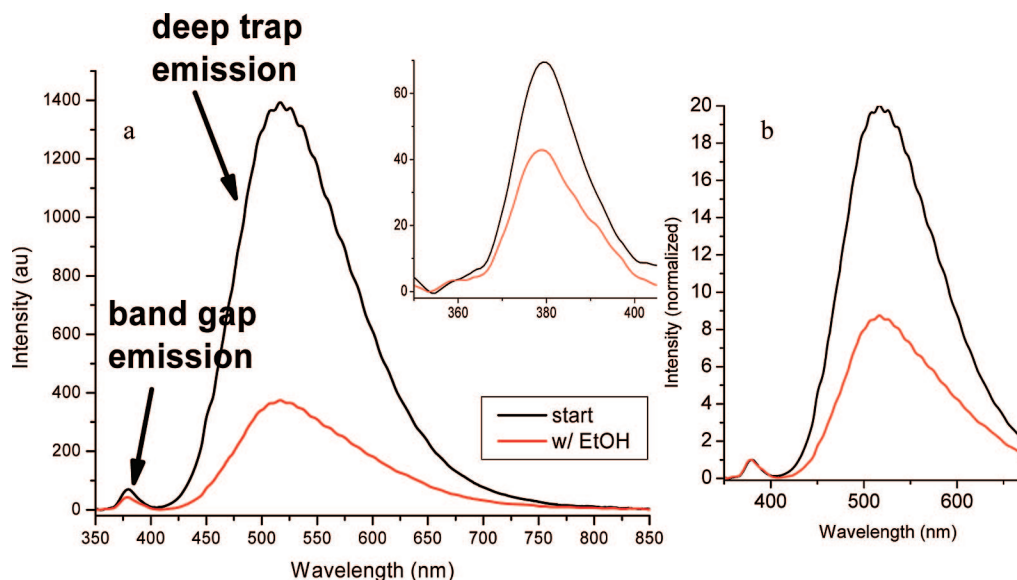


Figure 3. (a) PL emission of ZnO NWs grown on copper grids with and without ethanol. (b) The same spectra normalized to the band gap emission. Ethanol is able to decrease the intensity of the deep trap emission and the band gap emission. The high intensity of the deep trap emission is due to the copper along the length of the NW.

sion and the remaining deep trap emission showing that there are multiple trapping mechanisms for excitons, not just surface traps.

The deep trap emission of ZnO has previously been attributed to a variety of different sources depending on the emission maximum. There has been a lot of disagreement regarding the source of emission in the green region. Singly ionized oxygen vacancies, antisite oxygen, oxygen vacancies, zinc vacancies, zinc interstitials, copper impurities, and surface defects have all been attributed as responsible for this emission.^{2,39,40} Differences in the temperature behavior, size of nanostructures, impurities, and growth conditions of ZnO structures suggest that multiple sources are responsible for similar emission.^{2,39,40} Previous measurements attribute the green trap emission to copper ions incorporated in the ZnO lattice, exhibiting fine structure at low temperature.⁴¹ Low-temperature cathodoluminescence measurements of these NWs⁴² show a green emission band with similar zero-phonon energy and fine structure to the band ascribed by Dingle to copper impurities. Our measurements thus suggest that the green emission band in these NWs arises, at least in part, from included copper ions.

As indicated, two other spectroscopic methods for compositional analysis, AES and EDS, were performed on the NW sample. EDS is used in a semiquantitative way to determine the bulk incorporation of copper into the NW samples. Figure 4a shows the area of interest, which is at a corner of the copper grid after ZnO NWs have been grown on the surface. In Figure 4b, the X-ray emission spectrum confirms the presence of copper, zinc, oxygen, and silicon. (The presence of silicon is due to the silicon wafer under the copper grid.) The emission spectrum is collected at every pixel, allowing el-

emental maps to be generated showing where that element is located in the field of view. The signals at 8.6 and 8.0 keV are used to generate the maps of zinc and copper shown in panels c and d of Figure 4, respectively. (The map of oxygen shows its presence everywhere due to the ZnO, the silica substrate, and the exposure of the whole surface to environmental oxygen and thus is not presented here.) The presence of both copper and zinc is observed over the copper grid, showing that a ZnO film forms on top of the copper grid. Since EDS is not surface specific, the copper atoms from the substrate underneath this ZnO film are also detected in this region. However, hanging off the edge of the copper grid, the zinc map clearly coincides with the SEM image of the NWs, confirming their composition. The copper map (Figure 4d) also shows intensity in the same regions as the NWs observed in panels a and c of Figure 4. This shows that copper is incorporated along the length of the growing ZnO NWs with slightly larger intensity corresponding to the tips of the NWs, further confirming the VLS mechanism.

Scanning AES is also performed on ZnO NW samples and their precursors in order to probe their composition and surface chemistry. Prominent AES features of bulk copper and zinc overlap.⁴³ In general, materials containing mixtures of atoms with overlapping spectra (such as the NWs of the present study) can only be properly analyzed using spectral stripping.⁴⁴ This process requires spectra collected from pure standards of each component in a chemical state equivalent to that of the sample (in this case, metal oxide NWs). Since the equivalent structures composed of purely copper oxide or zinc oxide are unknown, the materials must be approximated using available reference materials. Figure 5a shows the spectra obtained from the ZnO pre-

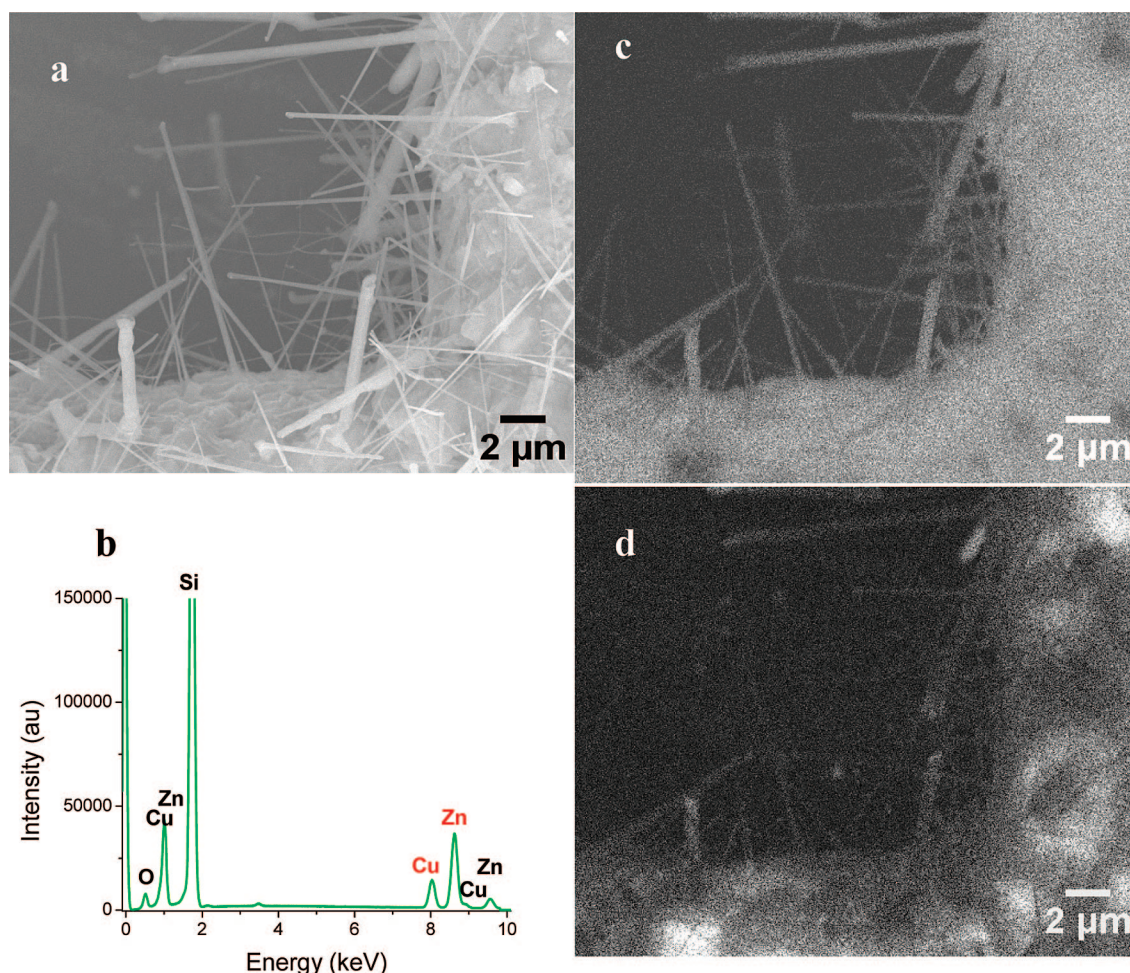


Figure 4. EDS images and spectrum of ZnO NWs grown on copper substrates. (a) SEM image of region showing NWs on a grid. (b) EDS spectrum of the imaged region. (Si signal is from the wafer beneath the Cu grid.) (c and d) Maps of Zn (8.6 keV) and Cu (8.0 keV) atoms in the sample, generated from the absorption peaks indicated in panel b, showing the presence of Zn and Cu atoms along the length of the NW, respectively. Note the increased Cu intensity centered at a number of the NW termini.

cursor and from an oxidized copper TEM grid. XRD confirmed that the copper oxide formed on the grid is Cu_2O (Figure S-2, Supporting Information). The LMM spectral features of Cu and Zn in these oxides confirm overlap at several energies between 750 and 950 eV.

AES spectra are collected at a series of points along the length of the NW, starting at the growth terminus, where according to the VLS mechanism a metallic copper droplet is expected to be observed. This area is shown in Figure 5b with the arrow representing the path followed for data acquisition. In order to separate the signal of the copper and zinc inside the NW, a spectral stripping procedure is used. Here, the stripping consists of derivatizing each spectrum, zero-centering about the baseline, normalizing to the largest Zn LMM feature (observed at 989 eV), then subtracting the zero-centered, normalized ZnO precursor spectrum from each NW spectrum. Figure 5c shows a representative AES derivative spectrum measured on the NW before stripping, normalized to the ZnO precursor spectrum from Figure 5a. The chemical similarity between the zinc spectra from the NW and the starting material is noted. Figure 5d shows the

normalized AES spectrum of the NW after ZnO stripping to obtain the copper signal from the NW along with the copper oxide spectrum. Comparison of the stripped NW spectra to the oxidized copper grid suggests that the Cu measured in the sample is chemically equivalent to the $(\text{Cu}^+)_2\text{O}$ found on the TEM grid, with its major peak at 918 eV. The features at 985 and 1008 eV remaining in stripped spectra in Figure 5d are due to slight chemical differences between the Zn in the ZnO precursor and the surface composition of the ZnO NW, which appears in this difference spectrum as enlarged features compared to Figure 5c.

The atomic fraction of C, O, Zn (using normalized raw data), and Cu (using the stripped spectra) are calculated in the usual way by utilizing published relative sensitivity factors (RSFs).⁴³ That is, the concentration C (in atom fraction) of element component x can be calculated as follows:

$$C_x = \frac{I_x / S_x}{\sum_{\alpha} (I_{\alpha} / S_{\alpha})} \quad (1)$$

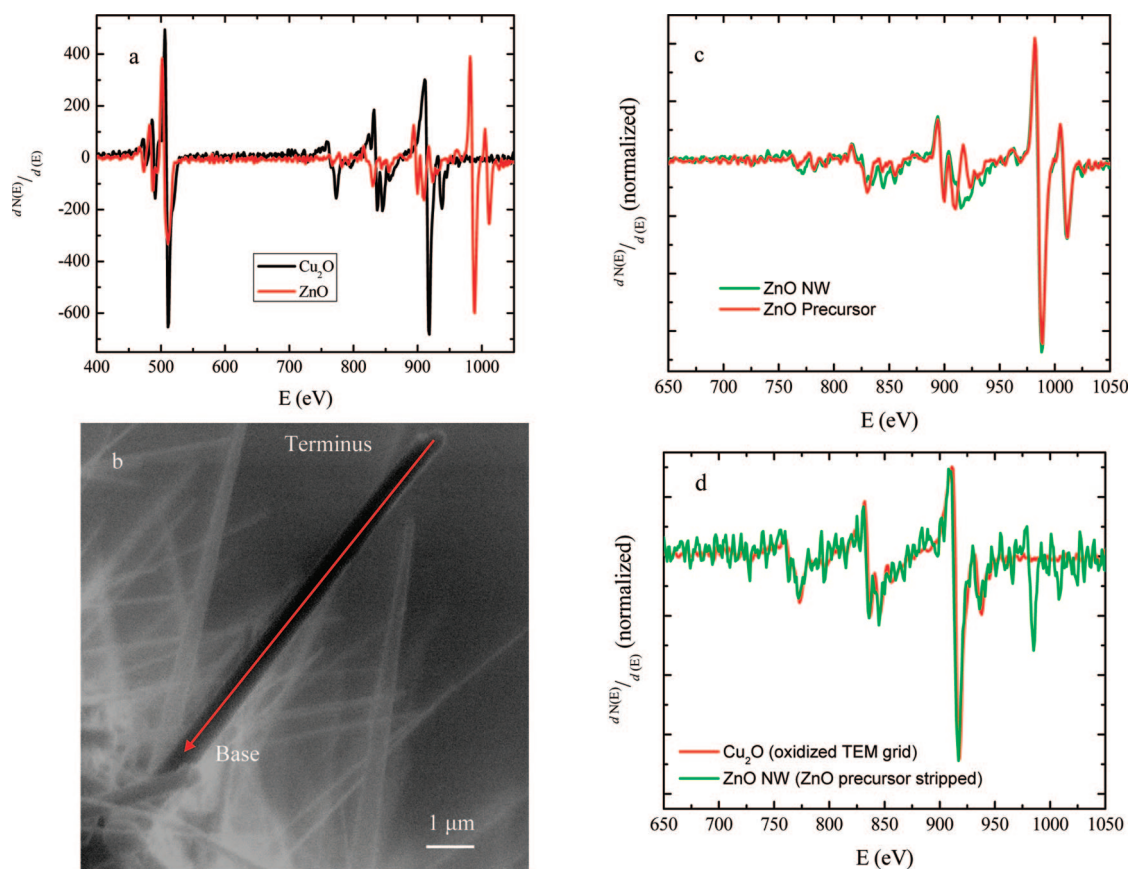


Figure 5. (a) Derivatized and zero-centered AES spectra of the ZnO precursor and oxidized copper (Cu_2O) TEM grid. The overlap of the LMM region (shown) obscures Cu signals, requiring spectral stripping to elucidate them. (b) Image of a representative NW (dark feature spanning diagonal) at $15000\times$ magnification. The AES profile line is noted (red). (c) NW spectrum, normalized to and superimposed over the ZnO precursor spectrum from Figure 5a. The Zn in the two samples is nearly chemically equivalent. (d) NW spectrum stripped of ZnO precursor spectrum showing the copper content of the NWs; the spectral coincidence of the oxidized copper TEM grid and the NW copper is evidence for chemical equivalence of copper in both samples. The features visible at 985 and 1008 eV are due to the slight chemical differences between the precursor ZnO and the ZnO NW.

where I_x is the amplitude of the derivative of a transition for element x , S_x is the RSF for x at the measured transition, and α is the set of elements in the sample. Figure 6 shows in graphical form the composition trend from the NW tip to its base obtained using eq 1 (with the literature values of the RSF). Equation 1 is also used

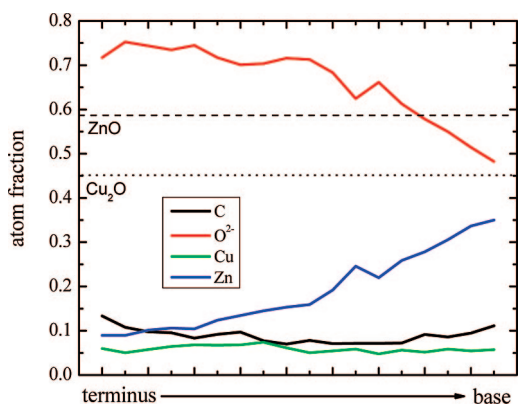


Figure 6. Compositional line profile of the NW from the terminus to the base using published RSFs for Cu and Zn. The dashed and dotted lines represent the Zn and Cu atomic fraction measured in their respective pure samples.

to calculate the percents of Zn and Cu in the reference materials using the literature RSF values for the metals. The calculated atomic fractions of Zn (58%) and Cu (45%) in the ZnO powder and the oxidized copper grid are shown as the dashed and dotted lines, respectively, in Figure 6. The spectral evidence in Figure 6 supports the formation of an oxygen-rich NW surface. This result is in agreement with previous work on ZnO surfaces that found that oxygen-terminated surfaces are more thermodynamically stable under long-term annealing.⁴⁵

Copper is detected along the entire length of the NW with only small variation in the atomic fraction along the NW. Moving from terminus to the base of the NW, the atomic fraction of oxygen on the surface decreases while the atomic fraction of zinc increases. While the relative surface concentration of Zn to Cu increases from the NW terminus to its base, at no point does AES measure the presence of purely metallic Cu (922 eV)⁴³ in the NW. In fact, the Cu concentration does not exceed an atom fraction of 8% assuming that RSFs for metals are valid for their ions.

We recomputed the RSFs of Zn and Cu by using the ZnO precursor and oxidized Cu from Figure 5a as reference data, assuming perfect sample stoichiometry, homogeneity, and equivalent bound O^{2-} . Inserting the recomputed RSFs (1.1012, 0.4717, and 1.5206 for O^{2-} , Cu^+ , and Zn^{2+} , respectively) into eq 1 generated the values shown in Figure S-3 (Supporting Information). While the trends in Figure S-3 are similar to those in Figure 6, the atomic fractions of Zn and O decrease while the atomic fraction of Cu increases. A maximum Cu atom fraction of 17% is obtained with the recalculated RSF values. The larger concentration of copper determined using the recomputed RSF values (Figure S-3) results in the concentration of the Zn and Cu crossing around the midpoint of the nanowire.

Traditionally, the drawing in Figure 1a is used to describe the structure of NWs grown by the VLS mechanism, where the metal is exclusively located at the terminus of the wire. For example, Wang and co-workers found that EDS detected only Au at the tip of ZnO NWs.⁴⁶ It is as significant to note that by using either of the RSFs (literature metallic or calculated ionic) described herein, there is a substantial copper concentration near the base of the NW (no less than 1:6 Cu:Zn, assuming metallic RSFs). Thus the copper is not remaining in the molten droplet as the NW is growing but is expelled as isolated copper ions along with the ZnO to form the NW. Also of note is the rather large zinc concentration measured at the terminus (no less than 4:9 Zn:Cu, assuming calculated ionic RSFs) showing that these materials remain alloys as the NW cools, leaving a mixed metal oxide coated droplet of copper of the NW tip.

METHODS

The ZnO NWs are grown by chemical vapor deposition in a high-temperature tube furnace. A small quartz tube (13 cm in length, 2.5 cm diameter) with a Si wafer in the middle containing a mixture of ground ZnO and graphite in a 1:1 mass ratio (≈ 0.15 g) is placed in the middle of the hot zone of the tube furnace. Downstream, a second Si wafer with a copper half TEM grid attached to the surface extends outside the small quartz tube. The tube furnace is set to ramp up to 890 °C at 100 °C/min and hold for 15 min with a continuous purge of argon at 0.60 standard L/min for a space velocity of 5 mm/s. The furnace initially reaches ≈ 1000 °C due to the high heating rate. The sample is allowed to cool in the tube furnace under argon flow until the temperature decreases below 400 °C, at which point the argon flow is stopped and the sample is removed from the furnace. An oxidized TEM grid was produced by following the same procedure without using any ZnO:graphite mixture, just residual oxygen; this method of producing a copper oxide reference sample for use in AES is similar to that used in prior work.⁴⁷

AES, TEM, SEM, XRD, EDS, and PL spectroscopy were all used to characterize the NWs generated. The TEM grid was used as both the substrate for NW growth and the source of copper while also providing a convenient means of indexing areas of interest on the sample. SEM images were obtained using a 5 kV acceleration voltage; AES was also performed at this incident beam energy with a 2 nA beam current, thus generating a nominal

CONCLUSIONS

Scanned probe electron microscopies and PL microscopy were employed to fully characterize ZnO NWs produced on a bulk copper catalyst. SEM data confirm particle size and position, while HR-TEM and XRD confirm structure and morphology with low structural defects. Taking into account the results from EDS and AES, it can be seen that the copper does not remain exclusively in the terminal droplet, as shown in the drawing in Figure 1a. The growth termini of the NWs contain copper and ZnO, showing that the alloying of these materials takes place in the droplet. Moreover, as is evident from both the PL data and the AES results, the copper is carried into the NW when the ZnO forms the NW. Due to the similarity of the copper AES reference spectrum and copper AES signal obtained from the NW, it appears that the copper is dispersed in the ZnO lattice as Cu^+ in isolated locations maintaining the bulk ZnO lattice observed in TEM images. The entire NW structure is apparently sheathed in an oxygen-rich mixed-metal oxide whose composition is dependent upon its distance from the growth terminus. The use of RSFs from either the literature values or the ionic species observed from reference samples gives similar qualitative pictures of these NWs. The oxygen-rich surface leads to increased deep trap emission. Copper ions that remain along the length of the NW are expected to lead to centers for recombination of charge carriers, leading to less intense band gap emission and more intense deep trap emission in the green as observed in the PL spectra for these samples. This analysis will be applied to other catalyst materials to determine if this is true of other metals or if it is due to a specific interaction between zinc and copper atoms.

spot size ≈ 23 nm. The total measurement time for each AES spectrum was ≈ 2.5 h. EDS was performed at 30 kV. TEM images were obtained using a 300 kV accelerating voltage. XRD spectra were obtained by tilting to a theta of 17° with a calibrated area detector and integrated over chi to obtain the spectrum shown.

A custom-built PL microscope was used to characterize the ZnO NWs optical properties. A HeCd laser operating at 325 nm was used to optically excite the ZnO NWs. The laser light was filtered with a Schott Glass UG11 filter to remove unwanted laser emission at 425 nm. (Commercial products identified here specify the means by which experiments were conducted. Such identification is not intended to imply recommendation or endorsement by the National Institute of Standards and Technology nor is it intended that the identified products are necessarily the best available for the purpose.) Five milliwatts of laser light was focused using a fused silica triplet lens onto an approximately 200 μ m diameter spot of the sample at a grazing angle. The ZnO PL was collected through an infinity corrected 40 \times objective with a numerical aperture of 0.60, which transmits wavelengths above 340 nm. Any residual scattered laser light from the sample was removed using a 6 optical density 325 nm laser blocking filter. The PL was then focused with a fused silica tube lens onto a charge couple device (CCD) camera used for focusing and imaging the area of interest. Once a suitable region was found, a mirror was placed into the microscope to direct the PL onto the face of a UV-transmitting fused silica fiber. The fiber

coupled the PL into a spectrometer coupled to a thermoelectrically cooled, scientific grade CCD for spectral acquisition. The wavelength sensitivity of the microscope and spectrometer system was measured using a tungsten halogen lamp as a reference source and an instrumental spectra response profile was generated. The spectral response of the PL microscope and spectrometer system was characterized in the range of 350–1100 nm. This spectral response data file was applied to all of the spectra presented here to account for the spectral sensitivity and though put of the instrument.

Supporting Information Available: Figures showing photoluminescence emission of ZnO NWs grown on copper grids with multiple exposures to EtOH, XRD of copper grid as received and after oxidation treatment, and compositional line profile of the NW using adjusted RSFs. This information is available free of charge via the Internet at <http://pubs.acs.org>.

REFERENCES AND NOTES

- Huang, M. H.; Mao, S.; Feick, H.; Yan, H.; Wu, Y.; Kind, H.; Weber, E.; Russo, R.; Yang, P. Room-Temperature Ultraviolet Nanowire Nanolasers. *Science* **2001**, *292*, 1897–1899.
- Djurisic, A. B.; Leung, Y. H. Optical Properties of ZnO Nanostructures. *Small* **2006**, *2*, 944–961.
- Yang, P.; Yan, H.; Mao, S.; Russo, R.; Johnson, J.; Saykally, R.; Morris, N.; Pham, J.; He, R.; Choi, H. J. Controlled Growth of ZnO Nanowires and Their Optical Properties. *Adv. Funct. Mater.* **2002**, *12*, 323–331.
- Johnson, J. C.; Yan, H.; Schaller, R. D.; Haber, L. H.; Yang, P.; Saykally, R. J. Single Nanowire Lasers. *J. Phys. Chem. B* **2001**, *105*, 11387–11390.
- Lee, C. J.; Lee, T. J.; Lyu, S. C.; Zhang, Y.; Ruh, H.; Lee, H. J. Field Emission from Well-Aligned Zinc Oxide Nanowires Grown at Low Temperature. *Appl. Phys. Lett.* **2002**, *81*, 3648–3650.
- Wang, X.; Jinhui Song, J. L.; Wang, Z. L. Direct-Current Nanogenerator Driven by Ultrasonic Waves. *Science* **2007**, *316*, 102–105.
- Zhao, M. H.; Wang, Z. L.; Mao, S. X. Piezoelectric Characterization of Individual Zinc Oxide Nanobelt Probed by Piezoresponse Force Microscope. *Nano Lett.* **2004**, *4*, 587–590.
- Huang, M. H.; Wu, Y.; Feick, H.; Tran, N.; Weber, E.; Yang, P. Catalytic Growth of Zinc Oxide Nanowires by Vapor Transport. *Adv. Mater.* **2001**, *13*, 113–116.
- Nikoobakht, B.; Michaels, C. A.; Stranick, S. J.; Vaudin, M. D. Horizontal Growth and in Situ Assembly of Oriented Zinc Oxide Nanowires. *Appl. Phys. Lett.* **2004**, *85*, 3244–3246.
- Yi, G.-C.; Wang, C.; Park, W. I. ZnO Nanorods: Synthesis, Characterization and Applications. *Semicond. Sci. Technol.* **2005**, *20*, S22–S34.
- Pan, Z. W.; Dai, Z. R.; Wang, Z. L. Nanobelts of Semiconducting Oxides. *Science* **2001**, *291*, 1947–1949.
- Dai, Y.; Zhang, Y.; Li, Q. K.; Nan, C. W. Synthesis and Optical Properties of Tetrapod-Like Zinc Oxide Nanorods. *Chem. Phys. Lett.* **2002**, *358*, 83–86.
- Yan, H.; He, R.; Pham, J.; Yang, P. Morphogenesis of One-Dimensional ZnO Nano- and Microcrystals. *Adv. Mater.* **2003**, *15*, 402–405.
- Yan, H.; He, R.; Johnson, J.; Law, M.; Saykally, R. J.; Yang, P. Dendritic Nanowire Ultraviolet Laser Array. *J. Am. Chem. Soc.* **2003**, *125*, 4728–4729.
- Wan, Q.; Li, Q. H.; Chen, Y. J.; Wang, T. H.; He, X. L.; Li, J. P.; Lin, C. L. Fabrication and Ethanol Sensing Characteristics of ZnO Nanowire Gas Sensors. *Appl. Phys. Lett.* **2004**, *84*, 3654–3656.
- Baxter, J. B.; Aydiel, E. S. Nanowire-Based Dye-Sensitized Solar Cells. *Appl. Phys. Lett.* **2005**, *86*, 053114/1–3.
- Garces, N. Y.; Wang, L.; Bai, L.; Giles, N. C.; Halliburton, L. E.; Cantwell, G. Role of Copper in the Green Luminescence from ZnO Crystals. *Appl. Phys. Lett.* **2002**, *81*, 622–624.
- Li, S. Y.; Lin, P.; Lee, C. Y.; Tseng, T. Y. Field Emission and Photofluorescent Characteristics of Zinc Oxide Nanowires Synthesized by a Metal Catalyzed Vapor-Liquid-Solid Process. *J. Appl. Phys.* **2004**, *95*, 3711–3716.
- Yamamoto, K.; Nagasawa, K.; Ohmori, T. Preparation and Characterization of ZnO Nanowires. *Physica E* **2004**, *24*, 129–132.
- Xu, C. X.; Sun, X. W.; Zhang, X. H.; Ke, L.; Chua, S. J. Photoluminescent Properties of Copper-Doped Zinc Oxide nanowires. *Nanotechnology* **2004**, *15*, 856–861.
- Li, S. Y.; Lin, P.; Lee, C. Y.; Tseng, T. Y. Effect of Atmosphere on Growth of Single Crystal Zinc Oxide Nanowires. *J. Mater. Sci.* **2004**, *15*, 505–510.
- Li, S. Y.; Lee, C. Y.; Tseng, T. Y. Copper-Catalyzed ZnO Nanowires on Silicon (100) Grown by Vapor-Liquid-Solid Process. *J. Cryst. Growth* **2003**, *247*, 357–362.
- Chiou, W.-T.; Wu, W.-Y.; Ting, J.-M. Effect of Electroless Copper on the Growth of ZnO Nanowires. *J. Mater. Res.* **2005**, *20*, 2348–2353.
- Zhou, S.-M.; Zhang, X.-H.; Meng, X.-M.; Zou, K.; Fan, X.; Wu, S.-K.; Lee, S.-T. The Fabrication and Optical Properties of Highly Crystalline Ultra-Long Cu-Doped ZnO Nanowires. *Nanotechnology* **2004**, *15*, 1152–1155.
- Yu, K.; Zhang, Y.; Luo, L.; Wang, W.; Zhu, Z.; Wang, J.; Cui, Y.; Ma, H.; Lu, W. Growth and Optical Properties of Quadrangular Zinc Oxide Nanorods on Copper-Filled Porous Silicon. *Appl. Phys. A: Mater. Sci. Process.* **2004**, *79*, 443–446.
- Wu, Y.; Yan, H.; Huang, M.; Messer, B.; Song, J. H.; Yang, P. Inorganic Semiconductor Nanowires: Rational Growth, Assembly, and Novel Properties. *Chem. Eur. J.* **2002**, *8*, 1260–1268.
- Fan, H. J.; Werner, P.; Zacharias, M. Semiconductor Nanowires: From Self-Organization to Patterned Growth. *Small* **2006**, *2*, 700–717.
- Kodambaka, S.; Tersoff, J.; Reuter, M. C.; Ross, F. M. Germanium Nanowire Growth Below the Eutectic Temperature. *Science* **2007**, *316*, 729–732.
- Khan, A.; Kordesch, M. E. Effect of Substrate Temperature on the Growth and Luminescence Properties of ZnO Nanostructures. *Physica E* **2005**, *30*, 51–54.
- Dalal, S.; Baptista, D.; Teo, K.; Lacerda, R.; Jefferson, D.; Milne, W. Controllable Growth of Vertically Aligned Zinc Oxide Nanowires Using Vapor Deposition. *Nanotechnology* **2006**, *17*, 4811–4818.
- Song, J. H.; Wang, X. D.; Riedo, E.; Wang, Z. L. Systematic Study on Experimental Conditions for Large-Scale Growth of Aligned ZnO Nanowires on Nitrides. *J. Phys. Chem. B* **2005**, *109*, 9869–9872.
- Givargizov, E. I. Fundamental Aspects of VLS Growth. *J. Cryst. Growth* **1975**, *31*, 20–30.
- Lee, G. H.; Jeon, H. D.; Lee, W. J.; Shin, B. C.; Kim, I. S. Fabrication of Chestnut Bur-Like Particles Covered with ZnO Nanowires. *J. Cryst. Growth* **2005**, *277*, 1–5.
- Zhu, Z.; Chen, T. L.; Gu, Y.; Warren, J.; Osgood, R. M., Jr. Zinc Oxide Nanowires Grown by Vapor-Phase Transport Using Selected Metal Catalysts: A Comparative Study. *Chem. Mater.* **2005**, *17*, 4227–4234.
- Park, K.; Lee, J.-S.; Sung, M.-Y.; Kim, S. Structural and Optical Properties of ZnO Nanowires Synthesized from Ball-Milled ZnO Powders. *Jpn. J. Appl. Phys.* **2002**, *41*, 7317–7321.
- Cotton, F. A.; Wilkinson, G. In *Advanced Inorganic Chemistry*, 5th ed.; John Wiley & Sons: New York, 1988; p 757.
- Wang, F.; Cao, L.; Pan, A.; Liu, R.; Wang, X.; Zhu, X.; Wang, S.; Zou, B. Synthesis of Tower-like ZnO Structures and Visible Photoluminescence Origins of Varied-Shaped ZnO Nanostructures. *J. Phys. Chem. C* **2007**, *111*, 7655–7660.
- Chen, Z. Q.; Wang, S. J.; Maekawa, M.; Kawasuso, A.; Naramoto, H.; Yuan, X. L.; Sekiguchi, T. Thermal Evolution of Defects in As-Grown and Electron-Irradiated ZnO Studied by Positron Annihilation. *Phys. Rev. B* **2007**, *75*, 245206/1–9.

39. Ozgur, U.; Ya, I. A.; Liu, C.; Teke, A.; Reshchikov, M. A.; Dogan, S.; Avrutin, V.; Cho, S. J.; Morkoc, H. A Comprehensive Review of ZnO Materials and Devices. *J. Appl. Phys.* **2005**, *98*, 041301/1–103.
40. Djuricic, A. B.; Choy, W. C. H.; Roy, V. A. L.; Leung, Y. H.; Kwong, C. Y.; Cheah, K. W.; Rao, T. K. G.; Chan, W. K.; Lui, H. F.; Surya, C. Photoluminescence and Electron Paramagnetic Resonance of ZnO Tetrapod Structures. *Adv. Funct. Mater.* **2004**, *14*, 856–864.
41. Dingle, R. Luminescent Transitions Associated with Divalent Copper Impurities and the Green Emission from Semiconducting Zinc Oxide. *Phys. Rev. Lett.* **1969**, *23*, 579–581.
42. Robins, L. H. Private communication, 2007.
43. Childs, K. D.; Carlson, B. A.; LaVanier, L. A.; Moulder, J. F.; Paul, D. F.; Stickle, W. F.; Watson, D. G. In *Handbook of Auger Electron Spectroscopy*, 3rd ed.; Hedberg, C., Ed.; Physical Electronics, Inc.: Eden Prairie, MN, 1995; p 404.
44. Grant, J. T.; Hooker, M. P.; Haas, T. W. Spectrum Subtraction Techniques in Auger Electron Spectroscopy. *Surf. Sci.* **1975**, *51*, 318–322.
45. Moller, P.; Komolov, S.; Lazneva, E.; Egebjerg, T. Oxygen Effect on the Conductivity of the $Cu_xO/ZnO(0001)$ and $(000\bar{1}\bar{1})$ Systems. *Appl. Surf. Sci.* **1999**, *142*, 210–214.
46. Wang, X. D.; Summers, C. J.; Wang, Z. L. Large-Scale Hexagonal-Patterned Growth of Aligned ZnO Nanorods for Nano-optoelectronics and Nanosensor Arrays. *Nano Lett.* **2004**, *4*, 423–426.
47. Panzner, G.; Egert, B.; Schmidt, H. P. The Stability of CuO and Cu_2O Surfaces During Argon Sputtering Studied by XPS and AES. *Surf. Sci.* **1985**, *151*, 400–408.